Zeeman effect in strong-field ionization

Jintai Liang [1], Yueming Zhou [1,*], Wei-Chao Jiang,[2,†] Miao Yu,[1] Min Li [1], and Peixiang Lu[1,3]

[1]*School of Physics and Wuhan National Laboratory for Optoelectronics, Huazhong University of Science and Technology, Wuhan 430074, China*
[2]*College of Physics and Optoelectronic Engineering, Shenzhen University, Shenzhen 518060, China*
[3]*Optics Valley Laboratory, Hubei 430074, China*

The magnetic effect on the bound state induced by the laser pulse is investigated in strong-field ionization. We find that the interaction of magnetic field of the laser pulse with atoms causes a time-dependent energy shift of the bound state, and the energy shift depends on the magnetic quantum numbers of the electrons, which is the so-called Zeeman effect. This time-dependent energy shift adds an extra phase to the tunneling electron wave packets. By solving the three-dimensional time-dependent Schrödinger equation, we demonstrate that this extra phase results in a shift of the interference structure originating from the interference of short and long trajectories of the backward-rescattering photoelectrons. The shift of the interference structure is also confirmed by simulations with the three-step model beyond the dipole approximation.

I. INTRODUCTION

With the development of laser technology, the amplitudes of the electric fields are on the order of the atomic binding field. Meanwhile, the magnetic components of the pulsed lasers are much stronger than the highest continuous field magnet in the world. For instance, the amplitude of the magnetic field is around 100 tesla for a laser pulse with the intensity of 10^{14} W/cm². However, in strong-field ionization, the effects of the magnetic fields of the laser pulses are rarely observed. This is because the ratio of the amplitudes for electric field and magnetic field equals the speed of light c, and thus the photoelectrons dynamics are mainly determined by the electric field. While in the high-intensity long-wavelength limit [1,2], the effects of the magnetic fields are non-negligible.

Specifically, the effect of the magnetic field shows up as an asymmetric photoelectron momentum distribution (PEMD) along the laser propagation direction (y axis in our work). The asymmetric PEMD results in a nonzero expectation value of p_y. In the high-intensity long-wavelength limit, this expectation value $\langle p_y \rangle$ can be formulated as $\langle p_y \rangle = (\langle E_k \rangle + I_p/3)/c$. Here, $\langle E_k \rangle$ and I_p are the average energies of the photoelectrons and binding energy of the initial state, respectively. The first term $\langle E_k \rangle /c$ results from the classical Lorentz force induced by the magnetic field acting on a free electron [3–5], and the additional term $I_p/3c$ originates from the action of the magnetic field on the electron during the tunneling ionization [6–10]. This effect has been demonstrated in experiments [11], nondipole time-dependent Schrödinger equation (TDSE) simulations [12], and nondipole strong-field approximation

(SFA) calculations [13,14]. When the rescattering electrons contribute to the PEMDs, the manifestation of the asymmetric PEMD is quite different. The magnetic field alters the rescattering process, leading to a backward-shifted narrow cusp in the PEMD along the laser propagation direction [15–21]. Additionally, the momentum transfer $\langle p_y \rangle$ from photon to the electrons strongly depends on the details of the scattering process. It is approximately given by $\langle p_y \rangle \approx \langle E_k \rangle /c$ for the photoelectrons with energies lower than $2U_p$ [11,21–23]. Here, $U_p = F_0^2/4\omega^2$ is the ponderomotive potential of the laser field with electric field amplitude F_0 and frequency ω. While for the electrons with energies beyond $2U_p$, the photon momentum transfer $\langle p_y \rangle$ remains constant as a function of $\langle E_k \rangle$ for He atom [23] and shows a V-shape structure for Xe atom [24].

As discussed above, previous works mainly focused on the magnetic effect on the ionized electron wave packets (EWPs), and this effect shows up in the laser propagation direction. However, it is still an open question of how the magnetic field affects the bound states and whether this effect is observable. One of the well-known magnetic effect on the bound states in the atoms is Zeeman effect [25], which has been deeply investigated in the static magnetic field. While for the magnetic field of the laser pulse, it oscillates with frequency of the laser pulse, and then the energy shift for the bound state induced by this magnetic field is time dependent. In the multicycle laser pulse, this time-dependent energy shift is smoothed out by the time averaging. Therefore, the Zeeman effect induced by the laser pulse can only be revealed by the subcycle electronic dynamics and it has not been observed up to now. Recent theoretical work has predicted that the Zeeman effect induced by the laser pulse can be observed in the Lyman-α transition in a hydrogen-like atom in a pulsed laser with the intensity up to 10^{20} W/cm² [26]. In strong-field ionization, the interference of the ionized EWPs encodes the information of the subcycle

*zhouymhust@hust.edu.cn
†jiang.wei.chao@szu.edu.cn

electronic dynamics, and thus the interference structures provide possible tools to reveal the Zeeman effect induced by the laser pulse with relatively lower intensity.

In this work, we investigate this time-dependent Zeeman effect on the interference structures originating from the interference of backward-rescattering photoelectrons with short and long trajectories. The backward-rescattering photoelectrons can reach energies up to $10U_p$ [27,28]. These high-energy electrons are at the heart of many well-known phenomena in strong-field physics, such as high-order harmonic generation [29–31] and laser-induced electron diffraction [32–35], which are both important for atomic and molecular imaging [35–37]. Mechanistically, the backward-rescattering photoelectrons with short and long trajectories are ionized at different times in the same one-quarter laser cycle [29,38]. Hence, the time-dependent energy shift induced by the magnetic field adds different initial phases to the short and long backward-rescattering electrons, which results in a shift of the interference structure. By solving the three-dimensional (3D) TDSE and simulating with the three-step model beyond the dipole approximation, we demonstrate the shift of the interference structures caused by the time-dependent Zeeman effect appearing in the PEMDs.

II. THEORY AND METHODOLOGY

The dynamics of an atom interacting with the laser pulses are governed by the TDSE, which in the velocity gauge is given by (atomic units are used unless otherwise stated [39])

$$i\frac{\partial}{\partial t}\Psi(\mathbf{r}, t) = H\Psi(\mathbf{r}, t), \tag{1}$$

with the Hamiltonian

$$H = \frac{[\mathbf{p} + \mathbf{A}(\mathbf{r}, t)]^2}{2} + V(\mathbf{r}). \tag{2}$$

Here, $\mathbf{A}(\mathbf{r}, t)$ is the vector potential of the laser pulse, and $V(\mathbf{r})$ is potential of the atom. Expanding the space-dependent vector potential to the first order in powers of $1/c$, the vector potential takes the approximate form

$$\mathbf{A}(\mathbf{r}, t) \simeq \mathbf{A}(t) + \frac{1}{c}(\hat{e} \cdot \mathbf{r})\mathbf{F}(t), \tag{3}$$

where $\mathbf{A}(t)$ represents the homogeneous vector potential, and $\mathbf{F}(t) = -d\mathbf{A}(t)/dt$ is the corresponding electric field. $\hat{e}$ is the unit vector along the laser propagation direction. By inserting Eq. (3) into Eq. (2), we express the lowest-order corrected non-dipole Hamiltonian as [40]

$$H_{\text{ND}} = \frac{1}{2}\mathbf{p}^2 + \mathbf{A}(t) \cdot \mathbf{p} + V(\mathbf{r}) + \frac{1}{c}(\hat{e} \cdot \mathbf{r})[\mathbf{A}(t) + \mathbf{p}] \cdot \mathbf{F}(t). \tag{4}$$

Note that here the purely time-dependent quadratic $\frac{1}{2}\mathbf{A}^2(t)$ term has been removed by the gauge transformation

$$\Psi' = \exp\left[i\int_{-\infty}^{t}\frac{1}{2}\mathbf{A}^2(\tau)d\tau\right]. \tag{5}$$

In our work, the laser pulse is linearly polarized along z axis and propagates along y axis. Then Eq. (4) is written as

$$H_{\text{ND}} = \underbrace{\frac{1}{2}p^2 + V(r)}_{H_0} + \underbrace{A(t)p_z}_{H_D^I} + \underbrace{\frac{1}{c}yA(t)F(t) + \frac{1}{c}yp_zF(t)}_{H_{\text{ND}}^I}. \tag{6}$$

To separate the magnetic effect from the nondipole correction Hamiltonian, we express term H_{ND}^I as

$$H_{\text{ND}}^I = \frac{1}{c}yA(t)F(t) + \underbrace{\frac{F(t)}{2c}L_x}_{H_{\text{MD}}} + \underbrace{\frac{F(t)}{2c}(yp_z + p_yz)}_{H_{\text{EQ}}}, \tag{7}$$

where the term yp_z is replaced by $yp_z = \frac{1}{2}(yp_z - p_yz) + \frac{1}{2}(yp_z + p_yz) = \frac{1}{2}L_x + \frac{1}{2}(yp_z + p_yz)$. Compared with the Hamiltonian in the length gauge [41–43], the terms H_{MD} and H_{EQ} represent the electric quadrupole (EQ) and magnetic dipole (MD) interaction, respectively.

In the past three decades, the electric quadrupole effect has been deeply studied in atomic photoionization [41,44–49]. Here, we focus on the magnetic dipole effect on the initial bound states. For the electrons that stay at the initial bound state $|nl_m^{\hat{L}}\rangle$ (n, l, m are the principal, angular, magnetic quantum numbers of the bound states and $\hat{L}$ represents the direction of the angular momentum), the energy shift induced by the magnetic field in the order of $1/c$ is written as

$$\Delta E_g(t) = \langle nl_m^{\hat{L}}|H_{\text{MD}}|nl_m^{\hat{L}}\rangle = \frac{1}{2}m\hat{L} \cdot \hat{e}_xB(t) \tag{8}$$

Here, $B(t) = F(t)/c$ is the magnetic field of the laser pulse. Apparently, the magnetic field induces a time-dependent energy shift of the initial state, which depends on the magnetic quantum number. This is the so-called Zeeman effect induced by the laser pulses. For a linearly polarized monochromatic laser pulse, $B(t) = B_0\cos(\omega t)$, the energy shifts induced by the magnetic fields for different initial states are illustrated in Figs. 1(a) and 1(b). It indicates that the energy shifts for $|2p_{-1}^x\rangle$ and $|2p_1^x\rangle$ states oscillate as the laser pulse in and out of phase. While for $|2p_0^x\rangle$ and $|2p_0^z\rangle$ states, there is no energy shift. Note that the energy shift induced by the other terms in Eq. (7) can be neglected, because

$$\langle nl_m^{\hat{L}}|\frac{1}{c}yA(t)F(t)|nl_m^{\hat{L}}\rangle = 0 \tag{9}$$

and

$$\langle nl_m^{\hat{L}}|H_{\text{EQ}}|nl_m^{\hat{L}}\rangle = -i\frac{F(t)}{2c}\langle nl_m^{\hat{L}}|yzH_0 - H_0yz|nl_m^{\hat{L}}\rangle = 0, \tag{10}$$

where the relations $p_z = -i[z, H_0]$ and $p_y = -i[y, H_0]$ are used. H_0 is the field-free Hamiltonian displayed in Eq. (6).

It is difficult to directly observe this small energy shift of the initial state. In strong-field ionization, this energy shift adds an extra phase to the ionized EWPs. Therefore, this time-dependent Zeeman effect can be revealed by the interference of the photoelectrons. The interference of two EWPs is described by

$$\mathcal{M}^2(\mathbf{p}) = |\mathcal{M}_1(\mathbf{p}) + \mathcal{M}_2(\mathbf{p})|^2 = |\mathcal{M}_1(\mathbf{p})|^2 + |\mathcal{M}_2(\mathbf{p})|^2 + 2|\mathcal{M}_1(\mathbf{p})||\mathcal{M}_2(\mathbf{p})|\cos(\mathcal{S}_2 - \mathcal{S}_1), \tag{11}$$
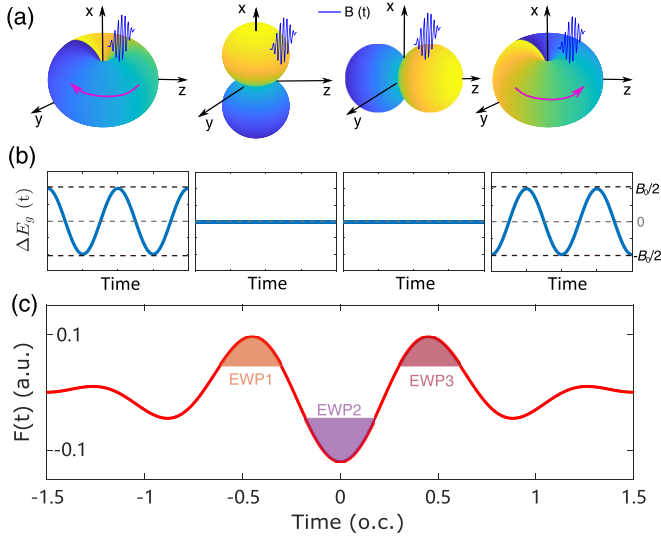
FIG. 1. (a) Illustration of ionization from different initial states with various magnetic quantum numbers. From left to right, the initial states are $|2p_{-1}^x\rangle$, $|2p_0^x\rangle$, $|2p_0^z\rangle$, $|2p_1^x\rangle$, respectively. The blue solid line represent the magnetic field of the laser pulse, which is polarized and propagates along the x and y axis, respectively. The corresponding electric field is polarized along z axis. (b) The time-dependent binding energy of the initial states induced by the magnetic field. (c) The electric field of the laser pulse used in our calculation. The shading areas with different colors indicate the ionization time of the tunneling EWPs contributing mostly to the PEMDs.

where $\mathcal{M}_i(\mathbf{p})$ and $\mathcal{S}_i$ are the ionization amplitudes and phase of the EWPs, respectively. With the SFA, the phase of the EWPs can be divided into two parts as [50]

$$\mathcal{S}_i = s_i + \int_{-\infty}^{t_i} E_g(t)dt = \underbrace{s_i - I_p t_i}_{\mathcal{S}_i^D} + \underbrace{\int_{-\infty}^{t_i} \Delta E_g(t)dt}_{\Delta \mathcal{S}_i} \quad (12)$$

Here s_i is the phase for the EWP accumulated in the laser pulse, and t_i is the ionization time of the EWP. $\Delta \mathcal{S}_i$ is the extra phase added by the time-dependent energy shift. For the two EWPs with the ionization times t_i^1 and t_i^2, the phase difference, which determines the interference structures, is written as

$$\mathcal{S}_2 - \mathcal{S}_1 = \left(\mathcal{S}_2^D - \mathcal{S}_1^D\right) + (\Delta \mathcal{S}_2 - \Delta \mathcal{S}_1)$$
$$= \left(\mathcal{S}_2^D - \mathcal{S}_1^D\right) + \frac{1}{2c}m\left[A(t_i^2) - A(t_i^1)\right]\hat{L} \cdot \hat{e}_x. \quad (13)$$

It implies that the time-dependent Zeeman effect will show up in the interference structures originating from the interference of the EWPs with different vector potential at the ionization time. In a linearly polarized laser pulse, the interference of the short and long trajectories of the backward-rescattering photoelectrons meets this condition. Moreover, these backward-rescattering electrons can reach energies of up to $10U_p$. Hence, it is easy to separate this interference structure from the PEMDs, which is beneficial to observe the time-dependent Zeeman effect on the initial states.

To demonstrate our scheme, we solve the 3D TDSE with the Hamiltonian shown in Eq. (4). In our calculation, the wavelength and intensity of the laser pulse are 800 nm and 5×10^{14} W/cm^2, respectively. The laser pulse is linearly

polarized along z axis and propagates along y axis, and its envelope has a cos-squared shape lasting three cycles. Figure 1(c) shows the electric field of the laser pulse. A recent investigation concluded that the nondipole effect of the backward-rescattering electrons sensitively depends on the model potential of the same atom [24]. To avoid this problem, we consider an one-electron system He$^+$, i.e., $V(r) = -2/r$. We solve the 3D TDSE in the spherical coordinates and the details of numerically solving TDSE have been shown in our previous works [51–54]. In our simulation, the angular momentum channels are chosen up to $L \leqslant 150$, $|M| \leqslant 20$. The time step is fixed at $\Delta t = 0.01$ a.u.. The maximal box size for the radial coordinate is chosen to be 600 a.u., and a mask function with a radius of 500 a.u. has been applied in each step of time propagation of the wave function. The convergence of our calculations has been confirmed by changing these parameters. The initial wave function is prepared by the imaginary-time propagation, which is chosen as the $|2p\rangle$ state of He$^+$ ion with the binding energy $I_p = 0.5$ a.u.. The ionization amplitude is extracted by projecting the final wave function to the scattering states of He$^+$ ion.

III. RESULTS AND DISCUSSION

Figure 2(a) shows the PEMD in the (p_x, p_z) plane (i.e., $p_y = 0$) from tunneling ionization of the $|2p_1^x\rangle$ state obtained by numerically solving the nondipole TDSE. The PEMD is symmetric about $p_x = 0$ and contains rich interference structures. These interference structures are deeply investigated in past decades [55–58]. Here, we focus on the photoelectrons with the energies larger than $2U_p$, which experience the backward rescattering with the parent ion. To reveal the ionization times of the backward rescattering electrons with different momenta, we adopt the three-step model to describe the motion of the photoelectrons [27,38]. As indicated by Fig. 1(c), there are three tunneling EWPs contributing mostly to the PEMD. In Fig. 2(a), we display the cutoff photoelectron momentum for these EWPs. The circles marked by I and II represent the results for the EWP1 when the rescattering occurs on the first and second time revisiting the parent ion, respectively. The circle marked by III is the result for the EWP2 rescattering with the parent ion at the first time revisiting. These results indicate that the photoelectrons with the large energies mainly stem from the backward rescattering of the EWP1. In this work, we concentrate on the ringlike structures locating $p_z < 0$. To trace origination of this type interference structure, we display the final energy of the backward-rescattering electrons of the EWP1 with the scattering angle $\theta_c = \pi$ as functions of the ionization time and rescattering time in Fig. 2(c). There are two ionization times for the electrons with the same final energy in one-quarter laser cycle, which are the so-called long and short trajectories [29,38]. The interference of the short and long trajectories displays the ringlike structures we focused on. For the PEMD from ionization of the $|2p_0^x\rangle$ state as shown in Fig. 2(b), this type interference structure is also clearly visible. Note that observation of the interference structure does not need the few-cycle laser pulse; it can also be observed in the multicycle laser pulse. We choose the three-cycle laser pulses to reduce the computational cost. We mention that the
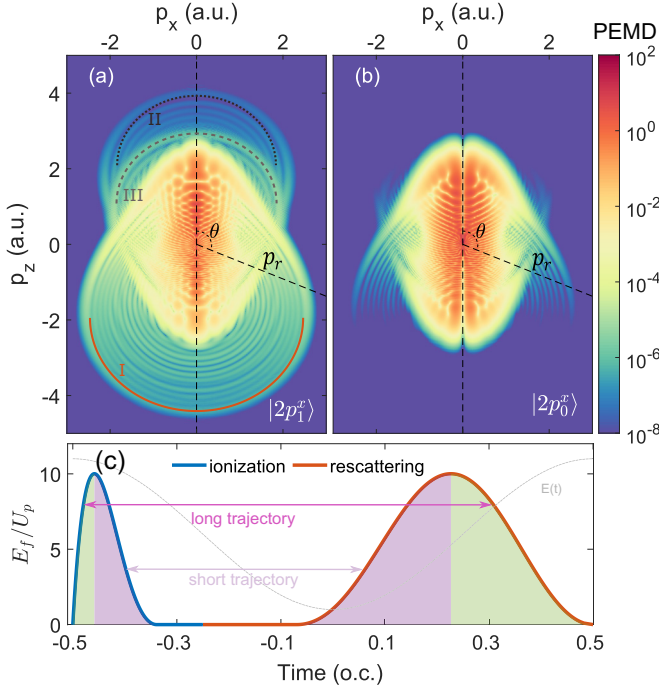
FIG. 2. (a) PEMD in the polarization plane from ionization of He$^+$ ion for $|2p_1^x\rangle$ state obtained by numerically solving the nondipole TDSE. The circles marked by I and II represent the cut off photoelectron momentum when the rescattering occurs on the first and second time, revisiting the parent ion of the EWP1 shown in Fig. 1(c). The circle marked by III is the momentum cutoff for the EWP2 rescattering at the first time revisiting the parent ion. (b) The same as (a) but for $|2p_0^x\rangle$ state. (c) The final energy of the backward-rescattering electrons with the scattering angle $\theta_c = \pi$ as functions of the ionization time (blue solid line) and rescattering time (red solid line), which are obtained by the three-step model. The ionization and rescattering time for the long and short trajectories are marked by the green and pink shading area, respectively.

PEMDs in Figs. 2(a) and 2(b) are different due to the initial state dependent transverse photoelectron phase structures of ionized EWPs [59].

The ringlike interference structures are analyzed in the polar coordinates in our work, as illustrated in Figs. 2(a) and 2(b). The cuts of the PEMDs at $\theta = 2$ rad are shown in Fig. 3. Figures 3(a) and 3(b) display the cuts of PEMDs from ionization of the $|2p_0^x\rangle$ and $|2p_0^z\rangle$ states, respectively, in which the solid and dashed lines represent the results for the dipole and nondipole TDSE calculations. Obviously, the solid and dashed lines are identical, which indicates that the nondipole interaction cannot affect the PEMDs in the polarization (p_x-p_z) plane for these two states in the laser pulse considered in our work. The reason for the same PEMDs in dipole and nondipole TDSE calculations is straightforward. As indicated by Eq. (8) and Fig. 1(b), the energy shifts induced by the time-dependent Zeeman effect are zero for these two states. Also, it has been demonstrated that the dynamics of the ionized electrons in p_x-p_z plane are the same with and without dipole approximation in the order of $1/c$ [22,23]. It implies that the nondipole interaction cannot affect the bound or the continuum states with $p_y = 0$ for these two initial
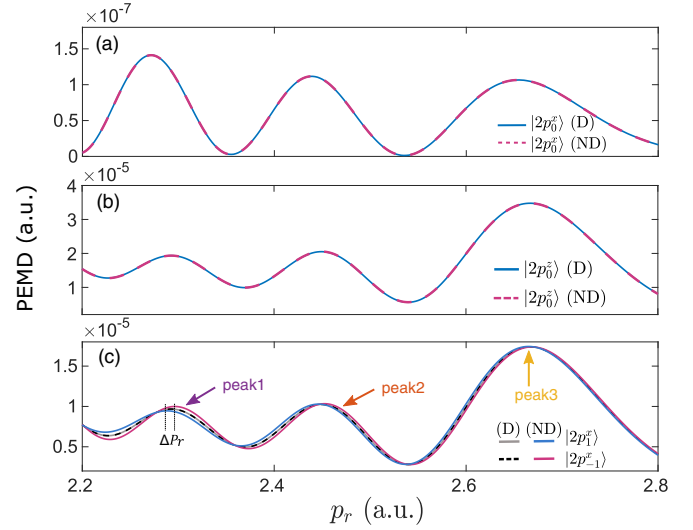

FIG. 3. [(a), (b)] Cuts of the PEMDs in the polar coordinates at $\theta = 2$ rad for $|2p_0^x\rangle$ and $|2p_0^z\rangle$ states, respectively. The solid and dashed lines are the results for the dipole (D) and nondipole (ND) TDSE calculations, respectively. (c) Same as (a) but for the $|2p_{\pm 1}^x\rangle$ states. The gray solid ($|2p_1^x\rangle$) and black dashed ($|2p_{-1}^x\rangle$) are the results for the PEMD obtained by numerically solving the TDSE with dipole approximation. The blue ($|2p_1^x\rangle$) and purple ($|2p_{-1}^x\rangle$) lines are the results for the nondipole TDSE calculation.

bound states. Thus, the PEMDs are the same for the dipole and nondipole TDSE.

However, for the $|2p_1^x\rangle$ and $|2p_{-1}^x\rangle$ states, as displayed in Fig. 3(c), the results for dipole and nondipole TDSE calculation are different. In the dipole TDSE calculations, as shown by the gray solid and black dashed lines, the PEMDs are the same for the $|2p_1^x\rangle$ and $|2p_{-1}^x\rangle$ states. It indicates that the AC-Stark shifts induced by the laser pulse are the same for these two states. While for the PEMDs obtained by nondipole TDSE calculations, the interference structure for the $|2p_1^x\rangle$ state shifts left with respect to the results of dipole TDSE, but it shifts right for the $|2p_{-1}^x\rangle$ state. Moreover, the shift of the interference structure decreases with p_r. For instance, the shift of peak 1 is larger than peak 2, and the shift disappears for peak 3. The shifts of the PEMDs originate from the Zeeman effect of the laser pulse. As suggested by Eq. (13), the time-dependent energy shifts of the initial states induced by the magnetic field add an extra phase difference between the short and long photoelectron trajectories, and the extra phase depends on the magnetic quantum number of the initial states and the ionization time intervals of the short and long photoelectron trajectories. The extra phase differences are opposite for $|2p_1^x\rangle$ and $|2p_{-1}^x\rangle$ states, which is responsible for the left shifted PEMD for $|2p_1^x\rangle$ and right shift for $|2p_{-1}^x\rangle$ states as displaced in Fig. 3(c). Furthermore, from analysis of the photoelectrons dynamics by the three-step model, the peak 3 corresponds to the cutoff momentum of the backward-rescattering electrons, where the ionization times of the short and long trajectories are the same as shown in Fig. 2(c). It implies that the ionization time intervals between the short and long trajectories decrease with p_r. Hence, the shift of the interference structure decreases with the radial momentum

of the photoelectrons. The above qualitative analysis of the TDSE results suggests that the time-dependent Zeeman effect caused by the magnetic components of the laser pulses can be revealed by the interference of the short and long photoelectron trajectories in strong-field ionization.

In order to further confirm that the shift of the interference structure originates from the Zeeman effect induced by the laser pulse, we also calculate the interference structures by the three-step model beyond the dipole approximation [22,23]. In this model, the potential-free acceleration of the photoelectrons is described classically by Newton's equation after tunneling ionization [50,60,61]. It has been demonstrated that the trajectories of the photoelectrons is only modified along the propagation direction of the laser pulse by the nondipole part of the Lorentz force in the first order of $1/c$ [22]. Therefore, the return condition in the polarization direction, $z(t_i) = z(t_r)$, is the same as it in the dipole approximation, which is written as

$$\int_{t_i}^{t_r} [\mathbf{A}(t) - \mathbf{A}(t_i)]dt = 0. \tag{14}$$

Here, t_i and t_r are the ionization and rescattering time, respectively. To map the final photoelectron momentum with the ionization time t_i and rescattering time t_r, we need the another condition, i.e., the photoelectron energy conservation before and after rescattering, which is given by [23]

$$\frac{\mathbf{p}^2}{2} + \left(1 + \frac{p_y}{c}\right)\left(\mathbf{p} \cdot \mathbf{A}(t_r) + \frac{1}{2}\mathbf{A}^2(t_r)\right)$$
$$= \frac{1}{2}[\mathbf{A}(t_r) - \mathbf{A}(t_i)]^2 + O\left(\frac{1}{c^2}\right). \tag{15}$$

In this work, we focus on the PEMD in the polarization plane, i.e., $p_y = 0$. So this condition is the same as it in the dipole approximation. It implies that the dynamics of the electrons in p_x-p_z plane is the same with and without nondipole correction in the order of $1/c$, and thus the motions of the electrons along p_y axis can be neglected. The phase for the EWP accumulated in the laser pulse s_i in Eq. (12) can be given by the classical action of the electrons as $s_i = \int_{t_i}^{+\infty} \mathbf{v}^2(t)/2$, where $\mathbf{v}(t)$ is momentum of the electron [50,60,61]. From classical analysis of the electrons motion by Eqs. (14) and (15), the photoelectron momentum before and after the rescattering is given by $\mathbf{v}(t < t_r) = \mathbf{A}(t) - \mathbf{A}(t_i)$ and $\mathbf{v}(t > t_r) = \mathbf{p} + \mathbf{A}(t)$, respectively. Therefore, the phase s_i for the photoelectron with final momentum of $\mathbf{p}$ is written as

$$s_i(\mathbf{p}) = \int_{t_i}^{t_r} \frac{1}{2}[\mathbf{A}(t) - \mathbf{A}(t_i)]^2 dt + \int_{t_r}^{+\infty} \frac{1}{2}[\mathbf{p} + \mathbf{A}(t)]^2 dt. \tag{16}$$

Note that we neglect the energy shifts of the continuum states caused by the nondipole effect, due to the adding term p_y/cU_p vanishing in the PEMD of the polarization plane ($p_y = 0$) [62–64]. Otherwise, when we consider the difference of the interference structures between $|2p_1^x\rangle$ and $|2p_{-1}^x\rangle$ states, the Stark effect can be neglected due to the same AC-Stark shifts for these two states as discussed above.

When we insert Eq. (16) into Eqs. (12) and (13), the phase difference for the short and long trajectories is obtained, and the interference structure $\cos^2[(\mathcal{S}_{long} - \mathcal{S}_{short})/2]$ for the
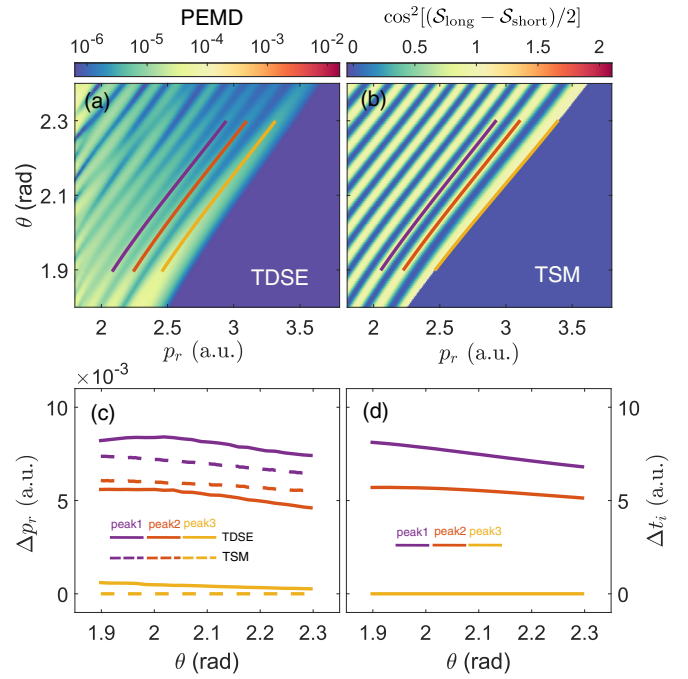

FIG. 4. (a) PEMD in the polar coordinates from ionization of He$^+$ ion for $|2p_1^x\rangle$ state obtained by numerically solving the nondipole TDSE. The solid lines represent the positions of interference maxima, and the lines with different colors correspond to the peaks marked by the arrows in Fig. 3(a). (b) The interference structures for the short and long backward-rescattering electron trajectories calculated by the three-step model (TSM) beyond dipole approximation. (c) The peak distance Δp_r between the results for $|2p_1^x\rangle$ and $|2p_{-1}^x\rangle$ states as a function of θ. The solid and dashed lines are the results obtained from the TDSE calculations and three-step model, respectively. The colors of lines correspond to the colors in panels (a) and (b). (d) The ionization time difference Δt_i between the short and long electron trajectories as a function of θ for the interference maxima shown in panel (b).

$|2p_1^x\rangle$ state is displayed in Fig. 4(b). Figure 4(a) shows the PEMD obtained by numerically solving TDSE for comparison. To qualitatively analyze the shift of the interference structure, we extract the peak positions of the interference structure as a function of θ as shown by the solid lines in Figs. 4(a) and 4(b). The lines with different colors correspond to the peaks marked by the arrows in Fig. 3(c). Then the peak distances Δp_r between the results of $|2p_1^x\rangle$ and $|2p_{-1}^x\rangle$ states [as indicated in Fig. 3(c)] as a function of θ are extracted, as displayed in Fig. 4(c). The solid and dashed lines represent the results obtained from the TDSE calculations and the three-step model, respectively. Obviously, the results obtained from these two methods reasonably coincide with each other, which suggests that the Zeeman effect induced by the laser pulse is successfully revealed by the interference of the backward-rescattering photoelectrons with short and long trajectories. Otherwise, the peak distances of peak 1 and peak 2 decrease with θ. To trace the origination of this trend of Δp_r, the ionization time intervals between the short and long photoelectron trajectories $\Delta t_i = t_i^{short} - t_i^{long}$ of the peak positions are displayed in Fig. 4(d). Here, t_i^{short} and t_i^{long} are

the ionization times of the short and long trajectories, respectively. As indicated by Eq. (13), the shift of the interference structure sensitively depends on the ionization time interval of the short and long trajectories, and the decreasing Δt_i as a function of θ is responsible for the decreasing of Δp_r.

IV. CONCLUSION

In conclusion, we have demonstrated that the Zeeman effect of the laser pulses can be revealed by the interference of the short and long trajectories of the backward-rescattering photoelectrons in strong-field ionization. The magnetic field of the laser pulse can induce different time-dependent energy shifts of the initial bound states, and this energy shift also depends on the magnetic quantum numbers of the electrons. Since the short and long trajectories are generated at the different times in the same one-quarter laser cycle, the time-dependent energy shifts of the initial states add different initial phases to the short and long photoelectron trajectories, which results in a shift of the interference structure. Our work first reveals the magnetic effect on the bound state induced by

the laser pulses in strong-field ionization and shows that the nondipole effect can show up in the PEMD of the polarization plane in theory.

Note that the Zeeman effect can also be observed in other atoms. We choose this simple atom to quantitatively illustrate our scheme. We also mentioned that the states with various magnetic quantum numbers can be prepared by exciting atom with particular polarized laser pulse [65,66]. Although observation of this effect is challenging in the experiment due to the laser focal averaging effect, it deepens our understanding of the magnetic field role and time-resolved photoelectron interference in strong-field ionization.

[1] H. R. Reiss, Limits on Tunneling Theories of Strong-Field Ionization, Phys. Rev. Lett. **101**, 043002 (2008).

[2] H. R. Reiss, The tunnelling model of laser-induced ionization and its failure at low frequencies, J. Phys. B **47**, 204006 (2014).

[3] C. T. L. Smeenk, L. Arissian, B. Zhou, A. Mysyrowicz, D. M. Villeneuve, A. Staudte, and P. B. Corkum, Partitioning of the Linear Photon Momentum in Multiphoton Ionization, Phys. Rev. Lett. **106**, 193002 (2011).

[4] A. S. Titi and G. W. F. Drake, Quantum theory of longitudinal momentum transfer in above-threshold ionization, Phys. Rev. A **85**, 041404(R) (2012).

[5] S. V. B. Jensen, M. M. Lund, and L. B. Madsen, Nondipole strong-field-approximation Hamiltonian, Phys. Rev. A **101**, 043408 (2020).

[6] M. Klaiber, E. Yakaboylu, H. Bauke, K. Z. Hatsagortsyan, and C. H. Keitel, Under-the-Barrier Dynamics in Laser-Induced Relativistic Tunneling, Phys. Rev. Lett. **110**, 153004 (2013).

[7] E. Yakaboylu, M. Klaiber, H. Bauke, K. Z. Hatsagortsyan, and C. H. Keitel, Relativistic features and time delay of laser-induced tunnel ionization, Phys. Rev. A **88**, 063421 (2013).

[8] B. Willenberg, J. Maurer, B. W. Mayer, and U. Keller, Subcycle time resolution of multi-photon momentum transfer in strong-field ionization, Nat. Commun. **10**, 5548 (2019).

[9] H. C. Ni, S. Brennecke, X. Gao, P. L. He, S. Donsa, I. Březinová, F. He, J. Wu, M. Lein, X. M. Tong, and J. Burgdörfer, Theory of Subcycle Linear Momentum Transfer in Strong-Field Tunneling Ionization, Phys. Rev. Lett. **125**, 073202 (2020).

[10] D. Cricchio, E. Fiordilino, and K. Z. Hatsagortsyan, Momentum partition between constituents of exotic atoms during laser-induced tunneling ionization, Phys. Rev. A **92**, 023408 (2015).

[11] A. Hartung, S. Eckart, S. Brennecke, J. Rist, D. Trabert, K. Fehre, M. Richter, H. Sann, S. Zeller, K. Henrichs, G. Kastirke, J. Hoehl, A. Kalinin, M. S. Schöffler, T. Jahnke, L. Ph H.

Schmidt, M. Lein, M. Kunitski, and R. Dörner, Magnetic fields alter strong-field ionization, Nat. Phys. **15**, 1222 (2019).

[12] S. Chelkowski, A. D. Bandrauk, and P. B. Corkum, Photon-momentum transfer in photoionization: From few photons to many, Phys. Rev. A **95**, 053402 (2017).

[13] S. Chelkowski, A. D. Bandrauk, and P. B. Corkum, Photon Momentum Sharing Between an Electron and an Ion in Photoionization: From One-Photon (Photoelectric Effect) to Multiphoton Absorption, Phys. Rev. Lett. **113**, 263005 (2014).

[14] P. L. He, D. Lao, and F. He, Strong Field Theories Beyond Dipole Approximations in Nonrelativistic Regimes, Phys. Rev. Lett. **118**, 163203 (2017).

[15] A. Ludwig, J. Maurer, B. W. Mayer, C. R. Phillips, L. Gallmann, and U. Keller, Breakdown of the Dipole Approximation in Strong-Field Ionization, Phys. Rev. Lett. **113**, 243001 (2014).

[16] J. Maurer, B. Willenberg, J. Daněk, B. W. Mayer, C. R. Phillips, L. Gallmann, M. Klaiber, K. Z. Hatsagortsyan, C. H. Keitel, and U. Keller, Probing the ionization wave packet and recollision dynamics with an elliptically polarized strong laser field in the nondipole regime, Phys. Rev. A **97**, 013404 (2018).

[17] J. Liu, Q. Z. Xia, J. F. Tao, and L. B. Fu, Coulomb effects in photon-momentum partitioning during atomic ionization by intense linearly polarized light, Phys. Rev. A **87**, 041403(R) (2013).

[18] J. Daněk, M. Klaiber, K. Z. Hatsagortsyan, C. H. Keitel, B. Willenberg, J. Maurer, B. W. Mayer, C. R. Phillips, L. Gallmann, and U. Keller, Interplay between Coulomb-focusing and non-dipole effects in strong-field ionization with elliptical polarization, J. Phys. B **51**, 114001 (2018).

[19] S. Chelkowski, A. D. Bandrauk, and P. B. Corkum, Photon-momentum transfer in multiphoton ionization and in time-resolved holography with photoelectrons, Phys. Rev. A **92**, 051401(R) (2015).

[20] S. Brennecke and M. Lein, Strong-field photoelectron holography beyond the electric dipole approximation: A semiclassical analysis, Phys. Rev. A **100**, 023413 (2019).

[21] B. Willenberg, J. Maurer, U. Keller, J. Daněk, M. Klaiber, N. Teeny, K. Z. Hatsagortsyan, and C. H. Keitel, Holographic interferences in strong-field ionization beyond the dipole approximation: The influence of the peak and focal-volume-averaged laser intensities, Phys. Rev. A **100**, 033417 (2019).

[22] S. Brennecke and M. Lein, High-order above-threshold ionization beyond the electric dipole approximation: Dependence on the atomic and molecular structure, Phys. Rev. A **98**, 063414 (2018).

[23] S. Brennecke and M. Lein, High-order above-threshold ionization beyond the electric dipole approximation, J. Phys. B **51**, 094005 (2018).

[24] K. Lin, S. Brennecke, H. Ni, X. Chen, A. Hartung, D. Trabert, K. Fehre, J. Rist, X. M. Tong, J. Burgdörfer, L. Ph. H. Schmidt, M. S. Schöffler, T. Jahnke, M. Kunitski, F. He, M. Lein, S. Eckart, and R. Dörner, Magnetic-Field Effect in High-Order Above-Threshold Ionization, Phys. Rev. Lett. **128**, 023201 (2022).

[25] C. Cohen-Tannoudji, B. Diu, and F. Laloë, *Quantum Mechanics* (Wiley, New York, 1977).

[26] E. Stambulchik and Y. Maron, Zeeman Effect Induced by Intense Laser Light, Phys. Rev. Lett. **113**, 083002 (2014).

[27] G. G. Paulus, W. Nicklich, H. Xu, P. Lambropoulos, and H. Walther, Plateau in Above Threshold Ionization Spectra, Phys. Rev. Lett. **72**, 2851 (1994).

[28] G. G. Paulus, W. Becker, W. Nicklich, and H. Walther, Rescattering effects in above-threshold ionization: A classical model, J. Phys. B **27**, L703 (1994).

[29] F. Krausz and M. Ivanov, Attosecond physics, Rev. Mod. Phys. **81**, 163 (2009).

[30] M. Ferray, A. L'Huillier, X. F. Li, L. A. Lompre, G. Mainfray, and C. Manus, Multiple-harmonic conversion of 1064 nm radiation in rare gases, J. Phys. B **21**, L31 (1988).

[31] P. M. Paul, E. S. Toma, P. Breger, G. Mullot, F. Augé, P. Balcou, H. G. Muller, and P. Agostini, Observation of a train of attosecond pulses from high harmonic generation, Science **292**, 1689 (2001).

[32] M. Lein, J. P. Marangos, and P. L. Knight, Electron diffraction in above-threshold ionization of molecules, Phys. Rev. A **66**, 051404(R) (2002).

[33] T. Morishita, A.-T. Le, Z. J. Chen, and C. D. Lin, Accurate Retrieval of Structural Information from Laser-Induced Photoelectron and High-Order Harmonic Spectra by Few-Cycle Laser Pulses, Phys. Rev. Lett. **100**, 013903 (2008).

[34] M. Okunishi, T. Morishita, G. Prümper, K. Shimada, C. D. Lin, S. Watanabe, and K. Ueda, Experimental Retrieval of Target Structure Information from Laser-Induced Rescattered Photoelectron Momentum Distributions, Phys. Rev. Lett. **100**, 143001 (2008).

[35] D. Ray, B. Ulrich, I. Bocharova, C. Maharjan, P. Ranitovic, B. Gramkow, M. Magrakvelidze, S. De, I. V. Litvinyuk, A. T. Le, T. Morishita, C. D. Lin, G. G. Paulus, and C. L. Cocke, Large-Angle Electron Diffraction Structure in Laser-Induced Rescattering from Rare Gases, Phys. Rev. Lett. **100**, 143002 (2008).

[36] C. I. Blaga, J. Xu, A. D. Dichiara, E. Sistrunk, K. Zhang, P. Agostini, T. A. Miller, L. F. Dimauro, and C. D. Lin, Imaging ultrafast molecular dynamics with laser-induced electron diffraction, Nature (London) **483**, 194 (2012).

[37] M. G. Pullen, B. Wolter, A.-T. Le, M. Baudisch, M. Hemmer, A. Senftleben, C. D. Schröter, J. Ullrich, R. Moshammer, C. D. Lin, and J. Biegert, Imaging an aligned polyatomic molecule with laser-induced electron diffraction, Nat. Commun. **6**, 7262 (2015).

[38] P. B. Corkum, Plasma Perspective on Strong Field Multiphoton Ionization, Phys. Rev. Lett. **71**, 1994 (1993).

[39] B. H. Bransden and C. J. Joachain, *Physics of Atoms and Molecules* (Prentice Hall, New York, 2003).

[40] M. Førre and A. S. Simonsen, Nondipole ionization dynamics in atoms induced by intense XUV laser fields, Phys. Rev. A **90**, 053411 (2014).

[41] J. W. Cooper, Photoelectron-angular-distribution parameters for rare-gas subshells, Phys. Rev. A **47**, 1841 (1993).

[42] R. Anzaki, Y. Shinohara, T. Sato, and K. L. Ishikawa, Gauge invariance beyond the electric dipole approximation, Phys. Rev. A **98**, 063410 (2018).

[43] A. Y. Istomin, N. L. Manakov, A. V. Meremianin, and A. F. Starace, Nondipole effects in the triply differential cross section for double photoionization of He, Phys. Rev. A **71**, 052702 (2005).

[44] P. Lambropoulos, G. Doolen, and S. P. Rountree, Electric Quadrupole Transitions in Multiphoton Ionization, Phys. Rev. Lett. **34**, 636 (1975).

[45] M. Lambropoulos, S. E. Moody, S. J. Smith, and W. C. Lineberger, Observation of Electric Quadrupole Transitions in Multiphoton Ionization, Phys. Rev. Lett. **35**, 159 (1975).

[46] B. Krässig, M. Jung, D. S. Gemmell, E. P. Kanter, T. LeBrun, S. H. Southworth, and L. Young, Nondipolar Asymmetries of Photoelectron Angular Distributions, Phys. Rev. Lett. **75**, 4736 (1995).

[47] V. K. Dolmatov and S. T. Manson, Enhanced Nondipole Effects in Low Energy Photoionization, Phys. Rev. Lett. **83**, 939 (1999).

[48] A. Hartung, S. Brennecke, K. Lin, D. Trabert, K. Fehre, J. Rist, M. S. Schöffler, T. Jahnke, L. P. H. Schmidt, M. Kunitski, M. Lein, R. Dörner, and S. Eckart, Electric Nondipole Effect in Strong-Field Ionization, Phys. Rev. Lett. **126**, 053202 (2021).

[49] G. Leuchs, S. J. Smith, S. N. Dixit, and P. Lambropoulos, Observation of Interference Between Quadrupole and Dipole Transitions in Low-Energy (2-eV) Photoionization from a Sodium Rydberg State, Phys. Rev. Lett. **56**, 708 (1986).

[50] M. Lewenstein, P. Balcou, M. Y. Ivanov, A. L'Huillier, and P. B. Corkum, Theory of high-harmonic generation by low-frequency laser fields, Phys. Rev. A **49**, 2117 (1994).

[51] W. C. Jiang and X. Q. Tian, Efficient split-Lanczos propagator for strong-field ionization of atoms, Opt. Express **25**, 26832 (2017).

[52] J. Liang, W. C. Jiang, S. Wang, M. Li, Y. Zhou, and P. Lu, Atomic dynamic interference in intense linearly and circularly polarized XUV pulses, J. Phys. B **53**, 095601 (2020).

[53] J. Liang, W. C. Jiang, Y. Liao, Q. Ke, M. Yu, M. Li, Y. Zhou, and P. Lu, Intensity-dependent angular distribution of low-energy electrons generated by intense high-frequency laser pulse, Opt. Express **29**, 16639 (2021).

[54] Q.-H. Ke, Y.-M. Zhou, Y.-J. Liao, J.-T. Liang, Y. Zhao, J. Tan, M. Li, and P.-X. Lu, Helicity-dependent time delays in

multiphoton ionization by two-color circularly polarized laser fields, Front. Phys. **16**, 52503 (2021).

[55] Y. Huismans, A. Rouzée, A. Gijsbertsen, J. H. Jungmann, A. S. Smolkowska, P. S. W. M. Logman, F. Lépine, C. Cauchy, S. Zamith, T. Marchenko, J. M. Bakker, G. Berden, B. Redlich, A. F. G. van der Meer, H. G. Muller, W. Vermin, K. J. Schafer, M. Spanner, M. Y. Ivanov, O. Smirnova *et al.*, Time-resolved holography with photoelectrons, Science **331**, 61 (2011).

[56] X. B. Bian, Y. Huismans, O. Smirnova, K. J. Yuan, M. J. J. Vrakking, and A. D. Bandrauk, Subcycle interference dynamics of time-resolved photoelectron holography with midinfrared laser pulses, Phys. Rev. A **84**, 043420 (2011).

[57] Y. Zhou, O. I. Tolstikhin, and T. Morishita, Near-Forward Rescattering Photoelectron Holography in Strong-Field Ionization: Extraction of the Phase of the Scattering Amplitude, Phys. Rev. Lett. **116**, 173001 (2016).

[58] J. Liang, Y. Zhou, J. Tan, M. He, Q. Ke, Y. Zhao, M. Li, W.C. Jiang, and P. Lu, Low-energy photoelectron interference structure in attosecond streaking, Opt. Express **27**, 37736 (2019).

[59] T. Bredtmann and S. Patchkovskii, Robust transverse structures in rescattered photoelectron wave packets and their observable consequences, Phys. Rev. A **99**, 063424 (2019).

[60] X. B. Bian and A. D. Bandrauk, Attosecond Time-Resolved Imaging of Molecular Structure by Photoelectron Holography, Phys. Rev. Lett. **108**, 263003 (2012).

[61] M. Li, J. Yuan, X. Sun, J. Yu, Q. Gong, and Y. Liu, Recollision-induced subcycle interference of molecules in strong laser fields, Phys. Rev. A **89**, 033425 (2014).

[62] S. Brennecke and M. Lein, Nondipole modification of the ac stark effect in above-threshold ionization, Phys. Rev. A **104**, L021104 (2021).

[63] K. Lin, S. Eckart, A. Hartung, D. Trabert, K. Fehre, J. Rist, L. Ph. H. Schmidt, M. S. Schöffler, T. Jahnke, M. Kunitski, and R. Dörner, Photoelectron energy peaks shift against the radiation pressure in strong-field ionization, Sci. Adv. **8**, eabn7386 (2022).

[64] M. M. Lund and L. B. Madsen, Nondipole photoelectron momentum shifts in strong-field ionization with mid-infrared laser pulses of long duration, J. Phys. B **54**, 165602 (2021).

[65] A. H. N. C. De Silva, D. Atri-Schuller, S. Dubey, B. P. Acharya, K. L. Romans, K. Foster, O. Russ, K. Compton, C. Rischbieter, N. Douguet, K. Bartschat, and D. Fischer, Using Circular Dichroism to Control Energy Transfer in Multiphoton Ionization, Phys. Rev. Lett. **126**, 023201 (2021).

[66] B. P. Acharya, M. Dodson, S. Dubey, K. L. Romans, A. H. N. C. De Silva, K. Foster, O. Russ, K. Bartschat, N. Douguet, and D. Fischer, Magnetic dichroism in few-photon ionization of polarized atoms, Phys. Rev. A **104**, 053103 (2021).